Supplementary data

A randomized controlled trial of GLP-1 receptor agonist dulaglutide in primary polydipsia

*Bettina Winzeler, MD[1,2], *Clara Odilia Sailer, MD-PhD[1,2], David Coynel, PhD[3,4], Davide Zanchi, PhD[5,6], Deborah R. Vogt, PhD[1,2,7], Sandrine Andrea Urwyler, MD[1,2], Julie Refardt, MD[1,2], Mirjam Christ-Crain, MD-PhD[1,2]

1 Department of Endocrinology, Diabetology and Metabolism, University Hospital Basel, Basel, Switzerland

2 Department of Clinical Research, University of Basel, Basel, Switzerland

3 Division of Cognitive Neuroscience, Department of Psychology, University of Basel, CH-4055 Basel, Switzerland

4 Transfaculty Research Platform, University of Basel, CH-4055 Basel, Switzerland

5 F. Hoffmann-La Roche, Roche Innovation Centre Basel, Basel, Switzerland

6 Stanford University Graduate School of Business, Stanford, CA

7 Clinical Trial Unit, University of Basel and University Hospital Basel, Basel, Switzerland

*equally contributing first authors

METHODS

Statistical analysis

The primary endpoint, and – unless indicated otherwise – all continuous secondary endpoints, were analyzed for a treatment effect (dulaglutide - placebo) using linear mixed-effect models (LMM). A random intercept was fitted for patient. To examine whether treatment sequence affected the outcome, we first fitted all statistical models with treatment (dulaglutide - placebo), treatment sequence (dulaglutide/placebo – placebo/dulaglutide) and the interaction term (treatment: treatment sequence) as explanatory variables. If available, the baseline measurement of the respective outcome was included as covariate. Since we found no indication for an interaction with treatment sequence for any reported outcome, all statistical models were refitted without treatment sequence and interaction term.

We further analyzed the possibility of a carryover/sequence effects on patient characteristics that have been assessed before/at the beginning of each treatment phase and in which such an effect might occur.

We report the estimated treatment effects with 95% confidence intervals computed using the likelihood profile method, whenever possible, or using the Wald method otherwise.

For the primary analysis we report a p-value which was calculated using the Satterwaite's method for deriving degrees of freedom and t-statistics.

(f)MRI acquisition

All (f)MRI acquisitions were performed on a Siemens MAGNETOM Prisma 3T scanner, equipped with a 20 channels head coil.

Anatomical images

At each MRI session (two treatment sessions for patients, one session for controls), a high-resolution T1-weighted anatomical image (T1w) was acquired using a magnetization prepared

gradient echo sequence (MPRAGE) with the following parameters: TR = 2000 ms; TE = 3.37 ms; TI = 1000 ms; flip angle = 8°; 176 saggital slices; FOV = 256 mm; voxel size = 1x1x1 mm3; anterior-to-posterior phase encoding direction; GRAPPA factor 2; no fat suppression; acquisition time 4min08s.

Functional images

Task fMRI

Whole-brain blood oxygen level-dependent fMRI was acquired using a single-shot echo-planar sequence (EPI). The following acquisition parameters were used: TE = 28 ms; TR = 2500 ms; flip angle = 82°; acquisition time 4min55s; 116 volumes; anterior-to-posterior phase encoding direction; no parallel imaging; interleaved ascending slice acquisition (first slice: #2); 40 axial slices; slice thickness 3 mm; interslice gap 0.51 mm (17%); FOV = 228 mm; acquisition matrix = 76x76; voxel size: 3×3×3 mm3.

Pictures of beverages (n = 24) and chairs (n = 24) were shown on uniform gray-colored background. Beverage and chair pictures were matched in terms of complexity, size and overall appearance and did not include commercial labels. Pictures were pseudorandomized in 10 sets (5 sets of chair and 5 sets of beverage) of 10 pictures, each picture shown for 2 seconds without interruption. After each set, patients had 4 seconds to rate their perceived thirst on a 7-point numerous rating scale. Beverage and chair pictures were matched in terms of complexity, size and overall appearance and did not include commercial labels.

Resting-state

Whole-brain blood oxygen level-dependent fMRI was acquired using a single-shot echo-planar sequence (EPI). The following acquisition parameters were used: TE = 28 ms; TR = 1800 ms; flip angle = 82°; acquisition time 5min08s; 168 volumes; anterior-to-posterior phase encoding direction; no parallel imaging; interleaved ascending slice acquisition (first slice: #1); 35 axial

slices; slice thickness 3.5mm; interslice gap 0.525 mm (15%); FOV = 224 mm; acquisition matrix = 64x64; voxel size: 3.5×3.5×3.5 mm3.

B0 field map

A B0 field map was acquired using dual-echo gradient-recall echo sequence. The following acquisition parameters were used: TE1 = 4.92 ms; TE2 = 7.38 ms; TR = 500 ms; flip angle = 50°; acquisition time1min07s; anterior-to-posterior phase encoding direction; interleaved slice acquisition; 35 axial slices; slice thickness 3.5 mm; interslice gap 0.525 mm (15%); FOV = 224 mm; acquisition matrix = 64x64; voxel size: 3.5×3.5×3.5 mm3.

(f)MRI preprocessing

Results included in this manuscript come from preprocessing performed using fMRIPrep 1.5.5 [1](RRID:SCR_016216), which is based on Nipype 1.4.0 [2] (RRID:SCR_002502). Calculations were performed at sciCORE (http://scicore.unibas.ch/) scientific computing center at University of Basel.

Anatomical data preprocessing

T1-weighted (T1w) images were corrected for intensity non-uniformity (INU) with N4BiasFieldCorrection [3], distributed with ANTs 2.2.0 [4] (RRID:SCR_004757). The T1w-reference was then skull-stripped with a Nipype implementation of the antsBrainExtraction.sh workflow (from ANTs), using OASIS30ANTs as target template. Brain tissue segmentation of cerebrospinal fluid (CSF), white-matter (WM) and gray-matter (GM) was performed on the brain-extracted T1w using fast (FSL 5.0.9, RRID:SCR_002823, (Zhang et al., 2001)). For the patients' data, a T1w-reference map was computed after registration of 2 T1w images (after INU-correction) using mri_robust_template (FreeSurfer 6.0.1, [5]). Brain surfaces were reconstructed using recon-all (FreeSurfer 6.0.1, RRID:SCR_001847 [6]), and the brain mask estimated previously was refined

with a custom variation of the method to reconcile ANTs-derived and FreeSurfer-derived segmentations of the cortical gray-matter of Mindboggle (RRID:SCR_002438) [7]. Volume-based spatial normalization to one standard space (MNI152NLin2009cAsym) was performed through nonlinear registration with antsRegistration (ANTs 2.2.0), using brain-extracted versions of both T1w reference and the T1w template. The following template was selected for spatial normalization: ICBM 152 Nonlinear Asymmetrical template version 2009c [8] (RRID:SCR_008796; TemplateFlow ID: MNI152NLin2009cAsym).

Functional data preprocessing

For each of the BOLD runs found per subject (across all tasks and sessions), the following preprocessing was performed. First, a reference volume and its skull-stripped version were generated using a custom methodology of fMRIPrep. A B0-nonuniformity map (or fieldmap) was estimated based on a phase-difference map calculated with a dual-echo GRE (gradient-recall echo) sequence, processed with a custom workflow of SDCFlows inspired by the epidewarp.fsl script and further improvements in HCP Pipelines [9]. The fieldmap was then co-registered to the target EPI (echo-planar imaging) reference run and converted to a displacements field map (amenable to registration tools such as ANTs) with FSL's fugue and other SDCflows tools. Based on the estimated susceptibility distortion, a corrected EPI (echo-planar imaging) reference was calculated for a more accurate co-registration with the anatomical reference. The BOLD reference was then co-registered to the T1w reference using bbregister (FreeSurfer) which implements boundary-based registration [10]. Co-registration was configured with six degrees of freedom. Head-motion parameters with respect to the BOLD reference (transformation matrices, and six corresponding rotation and translation parameters) are estimated before any spatiotemporal filtering using mcflirt (FSL 5.0.9) [11]. BOLD runs were slice-time corrected using 3dTshift from AFNI 20160207 (RRID:SCR_005927) [12]. The BOLD time-series were resampled to surfaces on the following spaces: fsaverage5. The BOLD time-series (including slice-timing correction when

applied) were resampled onto their original, native space by applying a single, composite transform to correct for head-motion and susceptibility distortions. These resampled BOLD time-series will be referred to as preprocessed BOLD in original space, or just preprocessed BOLD. The BOLD time-series were resampled into standard space, generating a preprocessed BOLD run in ['MNI152NLin2009cAsym'] space. First, a reference volume and its skull-stripped version were generated using a custom methodology of fMRIPrep. Several confounding time-series were calculated based on the preprocessed BOLD: framewise displacement (FD), DVARS and three region-wise global signals. FD and DVARS are calculated for each functional run, both using their implementations in Nipype (following the definitions by [13]. The three global signals are extracted within the CSF, the WM, and the whole-brain masks. Additionally, a set of physiological regressors were extracted to allow for component-based noise correction (CompCor[14]). Principal components are estimated after high-pass filtering the preprocessed BOLD time-series (using a discrete cosine filter with 128s cut-off) for the two CompCor variants: temporal (tCompCor) and anatomical (aCompCor). tCompCor components are then calculated from the top 5% variable voxels within a mask covering the subcortical regions. This subcortical mask is obtained by heavily eroding the brain mask, which ensures it does not include cortical GM regions. For aCompCor, components are calculated within the intersection of the aforementioned mask and the union of CSF and WM masks calculated in T1w space, after their projection to the native space of each functional run (using the inverse BOLD-to-T1w transformation). Components are also calculated separately within the WM and CSF masks. For each CompCor decomposition, the k components with the largest singular values are retained, such that the retained components' time series are sufficient to explain 50 percent of variance across the nuisance mask (CSF, WM, combined, or temporal). The remaining components are dropped from consideration. The head-motion estimates calculated in the correction step were also placed within the corresponding confounds file. The confound time series derived from head motion estimates and global signals were expanded with the inclusion of temporal derivatives and quadratic terms for

each [15]. Frames that exceeded a threshold of 1.0 mm FD or 1.5 standardised DVARS were annotated as motion outliers. All resamplings can be performed with a single interpolation step by composing all the pertinent transformations (i.e. head-motion transform matrices, susceptibility distortion correction when available, and co-registrations to anatomical and output spaces). Gridded (volumetric) resamplings were performed using antsApplyTransforms (ANTs), configured with Lanczos interpolation to minimize the smoothing effects of other kernels (Lanczos, 1964). Non-gridded (surface) resamplings were performed using mri_vol2surf (FreeSurfer).

Many internal operations of fMRIPrep use Nilearn 0.6.0 [16], RRID:SCR_001362), mostly within the functional processing workflow. For more details of the pipeline, see the section corresponding to workflows in fMRIPrep's documentation.

Preliminary quality control

Anatomical data

Brain mask, brain tissue segmentation and spatial normalization of the T1w data were visually inspected through fmriprep's visual quality assessment reports.

Functional data

Confounds estimated for the BOLD series were visually inspected through fmriprep's visual quality assessment reports: average global signals ('GlobalSignal', 'WM', 'GM'), standardized DVARS ('stdDVARS'), framewise-displacement ('FramewiseDisplacement'), and a 'carpetplot' summarizing the BOLD series. None of the subjects had more than 5 volumes with a framewise-displacement greater than 1 mm, across all tasks and sessions.

fMRI statistical modeling and inference

GOLD task

FMRI data statistical modeling was carried out using FEAT (FMRI Expert Analysis Tool) Version 6.00, part of FSL (FMRIB's Software Library, www.fmrib.ox.ac.uk/fsl).

Subject-level analyses

The following pre-statistics processing were applied: spatial smoothing using a Gaussian kernel of FWHM 6mm; grand-mean intensity normalisation of the entire 4D dataset by a single multiplicative factor; highpass temporal filtering (Gaussian-weighted least-squares straight line fitting, with sigma=50.0s).

Time-series statistical analysis was carried out using FILM with local autocorrelation correction [17]. The following explanatory variables (EVs) were included: chair stimulus presentation (5 blocks of 20s each), beverage stimulus presentation (5 blocks of 20s each), visual analog scale ratings (10 blocks of 4s each). Baseline was not explicitly modeled. Each event was convolved with the standard gamma haemodynamic response function. Twelve additional confound EVs from the fmriprep pipeline were added to the model: translation estimates (x, y, z), rotation estimates (x, y, z), quadratic translation estimates (x, y, z), quadratic rotation estimates (x, y, z). The temporal filtering option was also selected.

The following contrasts of interest were estimated for each subject and session: Chair, Beverage, Beverage>Chair, Chair>Beverage.

Group-level analyses

Stimuli: treatment interaction in patients

Single-subject contrast estimates for Beverage>Chair and Chair>Beverage in both treatment sessions were considered for a group-level interaction analysis. Each contrast was compared between treatment sessions with a mixed-effects approach using FLAME stage 1 [18–20] to test for

a stimuli : treatment interaction (paired two-group difference model). Z (Gaussianised T/F) statistic images were thresholded non-parametrically using clusters determined by Z>3.1 and a (corrected) cluster significance threshold of P=0.025 [21], to account for the two tested contrasts.

Stimuli: group interaction

Single-subject contrast estimates for Beverage>Chair and Chair>Beverage for the controls and placebo session for patients were considered for a group-level interaction analysis. Each contrast was compared between group with a mixed-effects approach using FLAME stage 1 [18–20] to test for a stimuli : group interaction (unpaired two-group difference model). Z (Gaussianised T/F) statistic images were thresholded non-parametrically using clusters determined by Z>3.1 and a (corrected) cluster significance threshold of P=0.025 [21], to account for the two tested contrasts.

Average contrasts across treatment sessions

Individual contrasts (Beverage>Chair; Chair>Beverage; Chair; Beverage) were combined across treatment sessions to create contrasts of parameter estimate (COPEs) for the subject means of each subject, using a fixed-effects analysis. Those estimates were then combined across subjects to obtain mean group effects, with a third-level mixed-effects analysis (one sample t-test). Z (Gaussianised T/F) statistic images were thresholded non-parametrically using clusters determined by Z>3.1 and a (corrected) cluster significance threshold of P=0.05 [21].

Resting-state

Time course extraction

Regions of interest (ROI) representing the reward network and the hypothalamus were selected based on previous findings [22]. A 6mm sphere was defined around the center coordinate of each region (supplementary table S4). The following 14 nuisance variables were extracted for each subject and session: global CSF and white matter signals; estimated translations and rotations in x/y/z directions; quadratic estimated translations and rotations in x/y/z directions.

Functional connectivity analyses

The following pre-statistics processing was applied; spatial smoothing using a Gaussian kernel of FWHM 6mm; grand-mean intensity normalisation of the entire 4D dataset by a single multiplicative factor; highpass temporal filtering (Gaussian-weighted least-squares straight line fitting, with sigma=50.0s). For each subject and session, the functional connectivity of each ROI was computed by means of a linear model, using FILM with local autocorrelation correction [17]. The included explanatory variables were the subject's ROI time course for that session, as well as the 14 nuisance variables.

Functional connectivity estimates were considered for group-level analyses. They were compared between treatment sessions in patients (paired two-group difference model), as well as between controls and patients under placebo (unpaired two-group difference model). Z (Gaussianised T/F) statistic images were thresholded non-parametrically using clusters determined by Z>3.1 and a (corrected) cluster significance threshold of P=0.05 [21].

High thirst state sub-group analysis

Patients that reported a median thirst rating of 5 or more during the placebo session were considered together with controls reporting a median thirst rating of 5 or more. This analysis aimed to describe the average activation pattern during the task. This group consisted of 14 patients and 10 controls. Mean group effects for the Beverage>Chair and Chair>Beverage contrasts were considered, by means of a mixed-effects analysis (one sample t-test). Z (Gaussianised T/F) statistic images were thresholded non-parametrically using clusters determined by Z>3.1 and a (corrected) cluster significance threshold of P=0.05 [21].

RESULTS

Quality of life

SF-12 physiological subscore, median [IQR], decreased slightly on dulaglutide from 55.2 [52.0, 56.1] to 52.7 [42.2, 55.9], while we observed no notable change on placebo: from 55.3 [48.0, 56.8] to 54.8 [49.6, 56.1]; baseline-adjusted estimated mean difference [95% CI]: -4.2 [-7.6, -0.9]. For the SF-12 mental subscore, however, we observed no change on dulaglutide, from 54.1 [44.8, 56.6] to 54.0 [45.8, 56.7], and a slight increase on placebo, from 51.0 [43.6, 55.9] to 53.8 [50.6, 56.4]; baseline-adjusted estimated mean difference [95% CI]: -1.0 [-3.8, 1.7].

Supplementary Tables

Table S1: Pre-treatment characteristics before start of placebo

	Placebo first	Dulaglutide first	p
n	17	18	
BMI (kg/m2)	23.0 [20.4, 25.1]	22.4 [20.4, 27.2]	0.830
BP systolic (mmHg)	124.4 (19.6)	121.6 (16.0)	0.639
BP diastolic (mmHg)	71.8 (6.2)	78.6 (7.6)	0.007
Heart rate	74.8 (12.2)	71.8 (12.6)	0.474
Serum sodium (mmol/l)	140.0 [138.0, 141.0]	140.0 [139.2, 141.0]	0.380
Urinary osmolality (mosm/kg)	452.0 [401.0, 560.0]	461.0 [274.2, 733.2]	0.692
Serum osmolality (mmol/l)	286.0 [285.0, 288.0]	286.5 [283.2, 293.8]	0.619
Fluid intake (ml)	4500.0 [4000.0, 5000.0]	4000.0 [3350.0, 5000.0]	0.097
Voiding frequency)	11.3 (4.2)	9.3 (4.5)	0.193
Drinking at night (no)	7 (41.2)	11 (61.1)	0.400
Nocturia (yes)	9 (52.9)	8 (44.4)	0.869

Table S2: Laboratory parameters on evaluation visit.

Blood parameters*	Placebo	Dulaglutide
Sodium (mmol/l), median (IQR)	140 (139-142)	140 (139-141)
Osmolality (mosm/kg), median (IQR)	289 (286-292)	286 (284-293)
Creatinine (mmol/l), median (IQR)	70 (62-81)	73 (62-82)
Urea (mmol/l), median (IQR)	4.15 (3.32-5.15)	3.85 (3.12-5.00)
Glucose (mmol/l), median (IQR)	4.80 (4.45-5.20)	4.40 (4.20-4.68)
24-hour urinary parameters		
Sodium (mmol/l), median (IQR)	38 (26-54)	40 (29-48)
Osmolality (mosm/kg), median (IQR)	217 (154-269)	245 (170-270)
Creatinine (mmol/l), median (IQR)	3.17 (1.86-4.10)	3.66 (2.46-5.04)
Urea (mmol/l), median (IQR)	188 (129-313)	209 (66-282)
Glucose (mmol/l), median (IQR)	0.1 (0-0.1)	0.1 (0-0.1)

*Blood taken at the start of the evaluation visit.

N = 34 each, except for serum glucose (n = 31 for placebo and n = 30 for dulaglutide) and urinary osmolality (n = 32 each).

Table S3: Gastrointestinal adverse effects

	Baseline	Week 1	Week 2	Week 3	Evaluation visit (morning)	Evaluation visit NRS
Gastrointestinal symptoms						
Nausea						
Dulaglutide	4 (11)	24 (71)	13 (38)	4 (11)	3 (9)	1 (1, 1.5)
Placebo	4 (11)	4 (11)	3 (9)	2 (6)	3 (9)	1 (1, 2)
Abdominal pain						
Dulaglutide	5 (15)	7 (21)	8 (24)	4 (11)	2 (6)	3 (3, 3)
Placebo	4 (11)	3 (9)	1 (3)	0 (0)	1 (3)	2 (2, 2)
Diarrhea						
Dulaglutide	2 (6)	2 (6)	6 (18)	1 (3)	1 (3)	
Placebo	1 (3)	1 (3)	2 (6)	1 (3)	1 (3)	
Vomitus						
Dulaglutide	0 (0)	7 (21)	3 (9)	0 (0)	0 (0)	
Placebo	0 (0)	0 (0)	0 (0)	0 (0)	0 (0)	
Other gastrointestinal symptoms*						
Dulaglutide	2 (6)	5 (15)	1 (3)	2 (6)	2 (6)	
Placebo	1 (3)	0 (0)	0 (0)	0 (0)	2 (6)	

*Other GIT symptoms: reflux/heartburn, constipation, flatulence. Abbreviations: NRS = Numerous rating scale

Data are shown as number (percentage) for each time point. The NRS indicates symptom severity as median (interquartile range) of patients who indicated an NRS > 0.

Table S4: Baseline characteristics of patients with primary polydipsia and matched controls (fMRI substudy).

	Primary Polydipsia	Matched Controls	p-value
Number of Patients	15	15	
Age (median [IQR])	32.0 [25.0, 39.5]	29.0 [24.5, 38.5]	0.901
Male Sex (%)	4 (27)	3 (20)	1.000
Alcohol per week (median [IQR])	1.0 [0.2, 4.0]	1.0 [0.0, 3.5]	0.833
Current Smoker (%)	6 (40)	5 (33)	1.000
Psychiatric disorder (%)	6 (40)	3 (20)	0.426
Depression (%)	2 (13)	3 (20)	1.000
Amount of Drinking, ml/d (median [IQR])	5000 [4250, 5500]	2000 [1500, 2000]	<0.001
Daytime emiction frequency, times/day (median [IQR])	10.0 [8.0, 13.0]	5.0 [4.0, 5.5]	<0.001

Continuous variables are expressed as median (interquartile range, IQR) and categorical variables as number (percentage, %).

Table S4: MNI coordinates of the seed regions used to compute functional connectivity

Region	x	y	z
Hypothalamus	0	-4	-12
Left accumbens	-14	10	-12
Right accumbens	13	10	-10
Midbrain	0	-18	-12

Supplementary Figures

Figure S1: Acute thirst perception during the evaluation visit

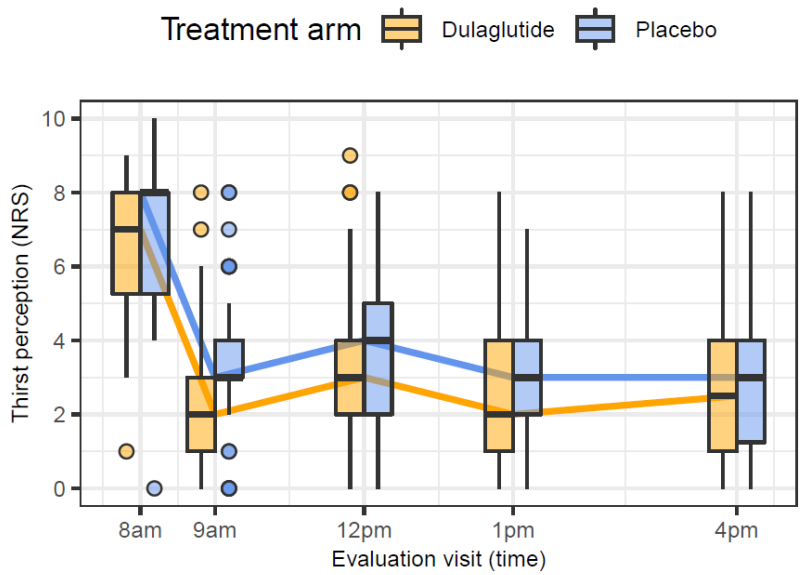

Time course of acute thirst perception (10-point numerous rating scale) during the evaluation visit for each treatment arm. Thick line indicates the median; box indicates the interquartile range (IQR); whiskers include all points within the range of 1.5x the IQR; dots represent all points outside 1.5x the IQR.

Figure S2: Individual treatment differences (dulaglutide-placebo) in serum sodium levels during the evaluation visit

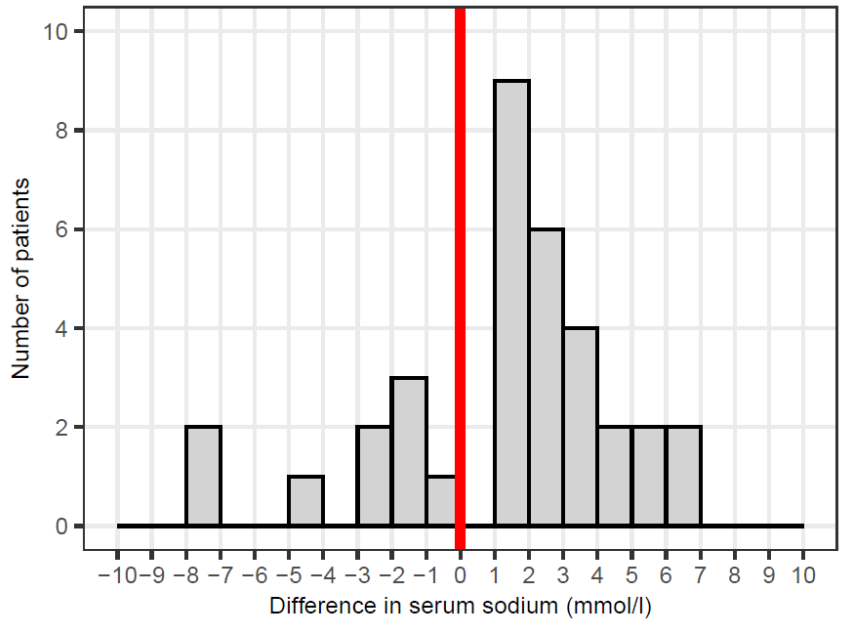

Differences of changes between the treatments (change dulaglutide - change placebo) of serum sodium within the 8 hours of the evaluation visit. Values > 0 indicate that there is a stronger increase or a lesser decline within 8 hours under dulaglutide as compared to placebo, which was the case for 25/34 patients

Figures S3: Individual treatment differences (dulaglutide-placebo) in urine osmolality during the evaluation visit

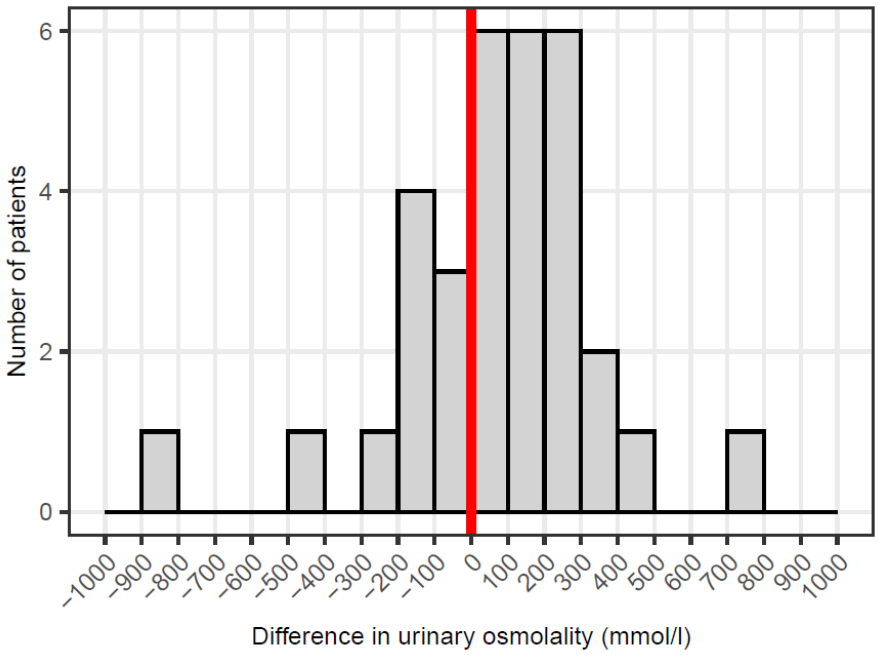

Differences of changes between the treatments (change dulaglutide - change placebo) of urine osmolality within the 8 hours of the evaluation visit. Values > 0 indicate that there is a stronger increase or a lesser decline within 8 hours under dulaglutide as compared to placebo, which was the case for 22/34 patients

Figure S4: Self-perceived nausea for each timepoint during the evaluation visit.

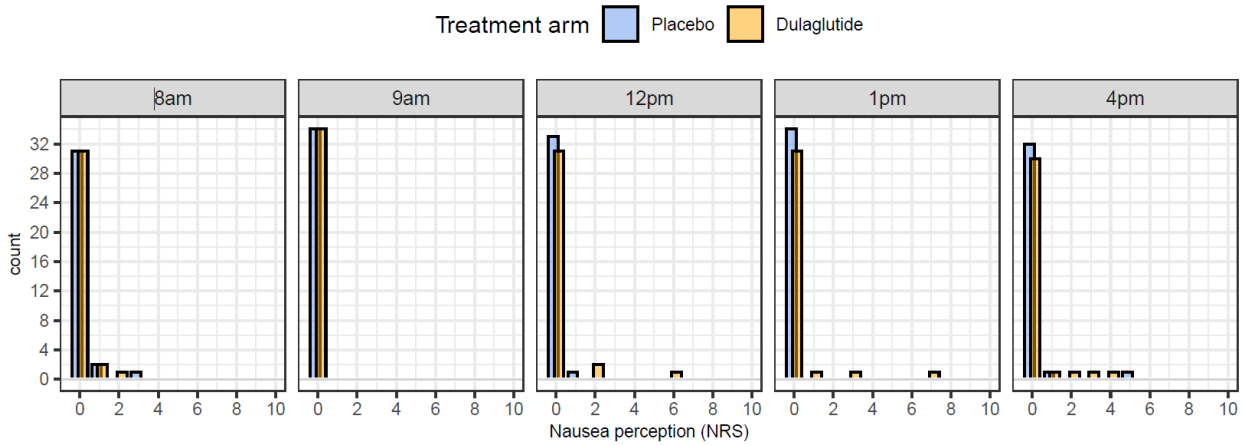

Patients were asked at the five timepoints during the evaluation visit (8:00 am, 9:00 am, noon, 1:00 pm, 4:00 pm) to indicate their acute self-perceived nausea on a 10-point numerous rating scale. Bar chart represent reported nausea for each patient and each timepoint.

Figure S5: Activation in patients on placebo (A) and dulaglutide (B), across stimuli.

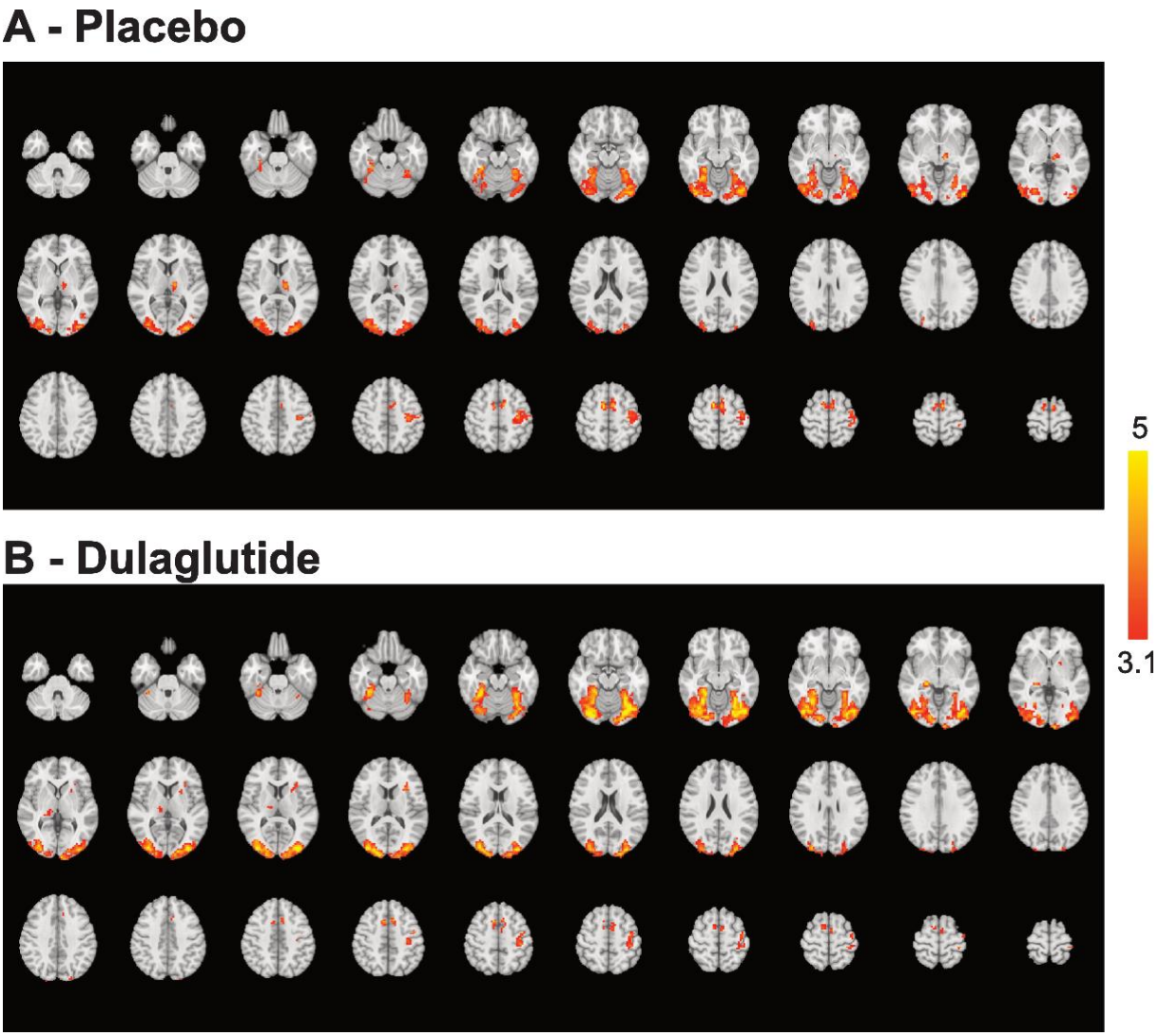

The colored overlay represents the Z-statistic values, after correction for multiple comparison at the whole-brain level. Similar activations within bilateral primary and secondary visual areas, the thalamus and right sensorimotor cortex were observed on dulaglutide and placebo.

Figure S6: Activation in high thirst ratings participants (patients under placebo and controls).

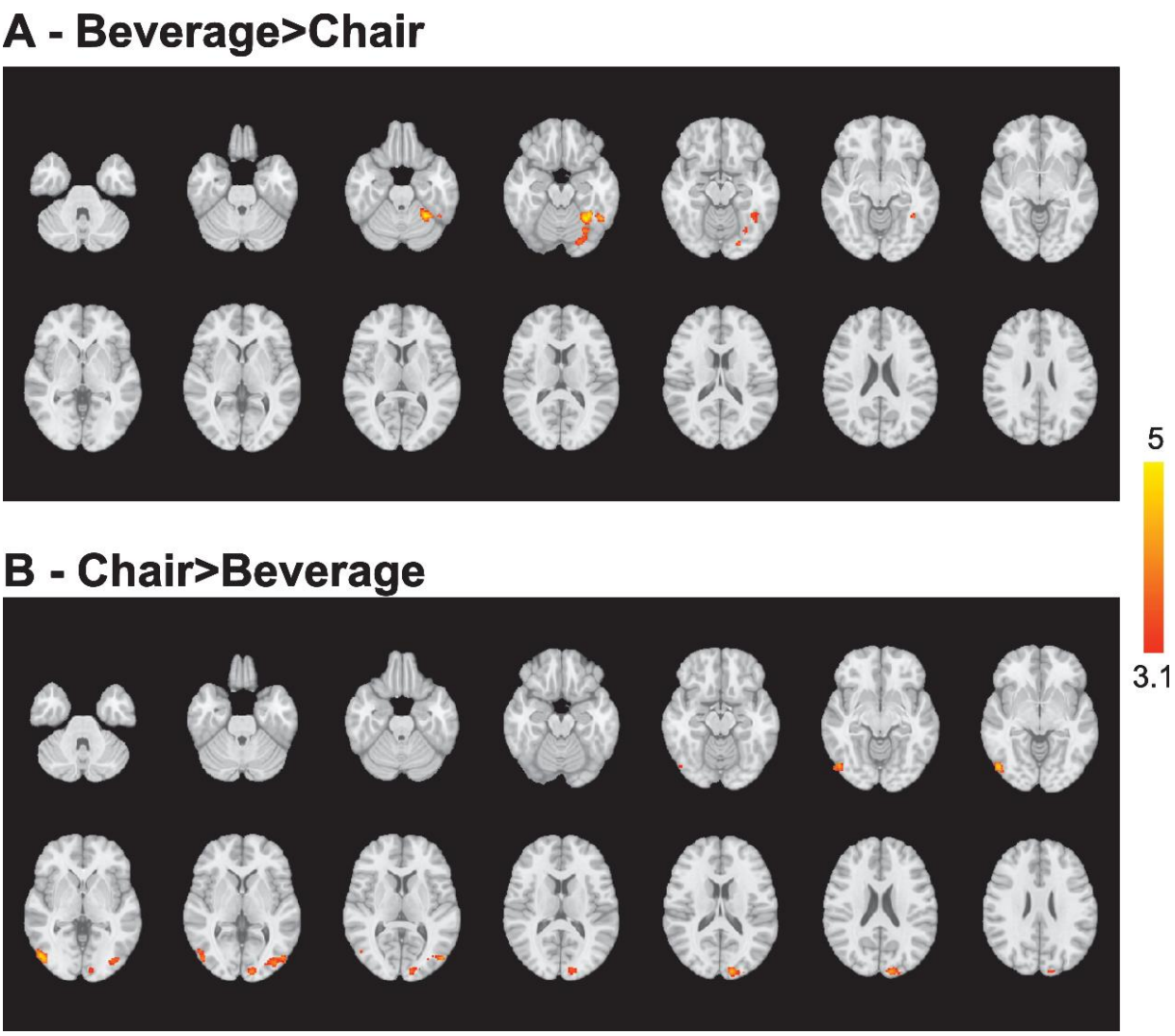

The colored overlay represents the Z-statistic values, after correction for multiple comparison at the whole-brain level. Several clusters of activation linked to visual processing were seen around the fusiform gyrus (A) and in the occipital lobe (B).

Figure S7: Activation across stimuli in patients under placebo (A) and controls (B).

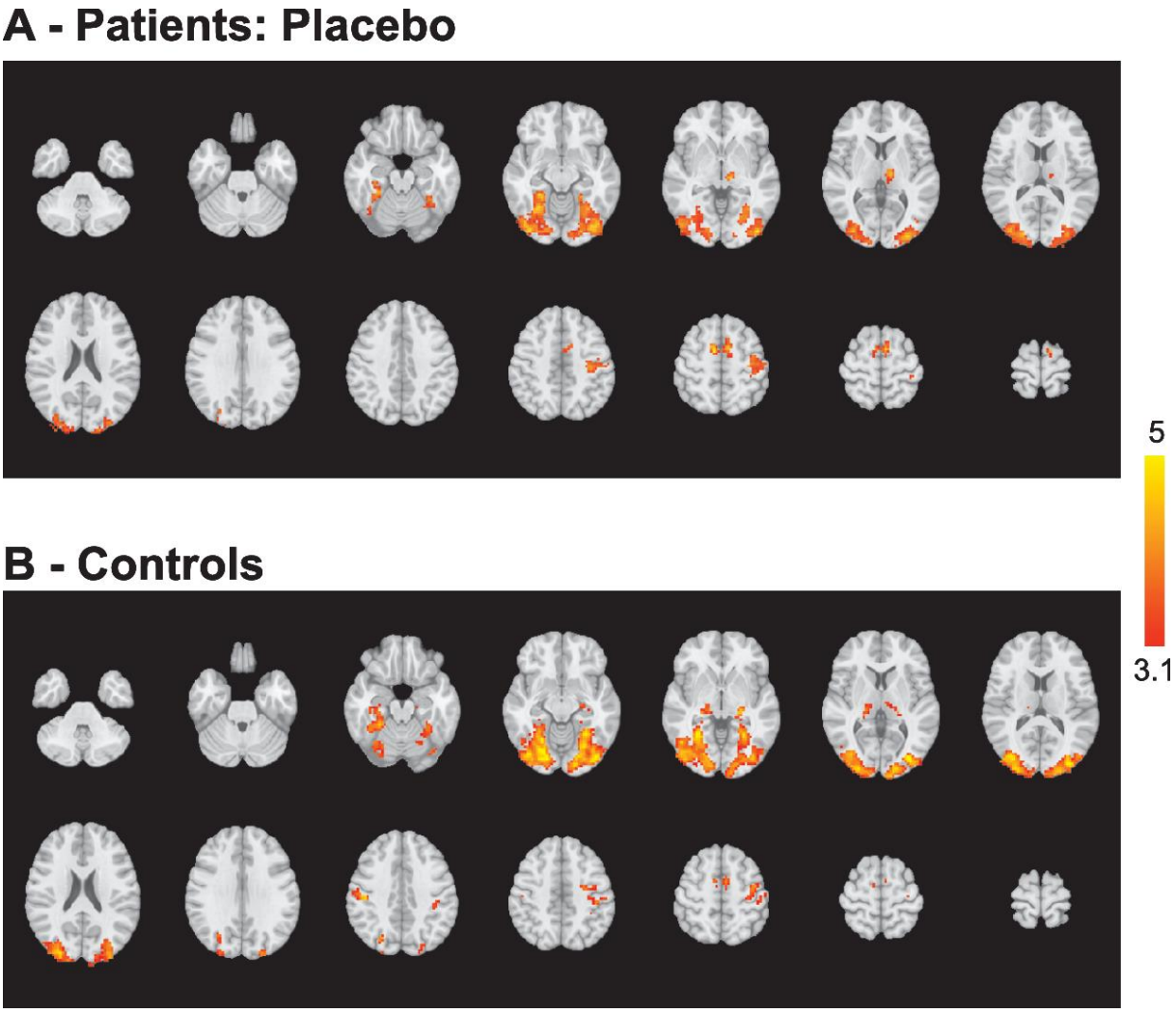

The colored overlay represents the Z-statistic values, after correction for multiple comparison at the whole-brain level. Similar activations within bilateral primary and secondary visual areas, the thalamus and right sensorimotor cortex were observed for both groups.

348 **Figure S8: Flow Chart**

349

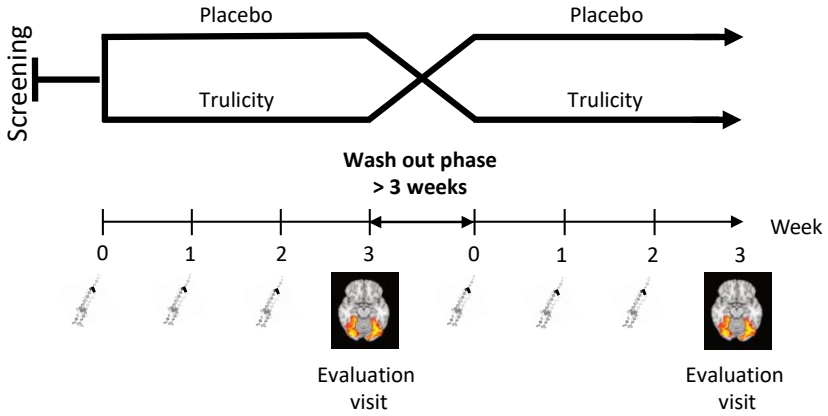

350

351

352
353

Figure S9: Seed regions used for the resting-state functional connectivity analyses.

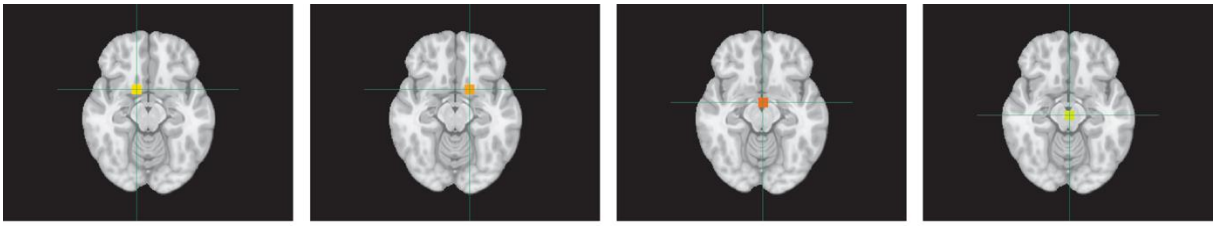

Right accumbens | Left accumbens | Hypothalamus | Midbrain

References

1. Esteban O, Markiewicz CJ, Blair RW, et al. fMRIPrep: a robust preprocessing pipeline for functional MRI. Nat Methods [Internet] 2019 [cited 2020 Nov 8];16(1):111–6. Available from: https://pubmed.ncbi.nlm.nih.gov/30532080/
2. Gorgolewski K, Burns CD, Madison C, et al. Nipype: A Flexible, Lightweight and Extensible Neuroimaging Data Processing Framework in Python. Front Neuroinform [Internet] 2011 [cited 2020 Nov 8];5:13. Available from: http://journal.frontiersin.org/article/10.3389/fninf.2011.00013/abstract
3. Tustison NJ, Avants BB, Cook PA, et al. N4ITK: Improved N3 bias correction. IEEE Trans Med Imaging [Internet] 2010 [cited 2020 Nov 8];29(6):1310–20. Available from: https://pubmed.ncbi.nlm.nih.gov/20378467/
4. Avants BB, Epstein CL, Grossman M, Gee JC. Symmetric diffeomorphic image registration with cross-correlation: Evaluating automated labeling of elderly and neurodegenerative brain. Med Image Anal [Internet] 2008 [cited 2020 Nov 8];12(1):26–41. Available from: https://pubmed.ncbi.nlm.nih.gov/17659998/
5. Reuter M, Rosas HD, Fischl B. Highly accurate inverse consistent registration: A robust approach. Neuroimage 2010;53(4).
6. Dale AM, Fischl B, Sereno MI. Cortical surface-based analysis: I. Segmentation and surface reconstruction. Neuroimage [Internet] 1999 [cited 2020 Nov 8];9(2):179–94. Available from: https://pubmed.ncbi.nlm.nih.gov/9931268/
7. Klein A, Ghosh SS, Bao FS, et al. Mindboggling morphometry of human brains. PLoS Comput Biol 2017;13(2).
8. Fonov V, Evans AC, Botteron K, Almli CR, McKinstry RC, Collins DL. Unbiased average age-appropriate atlases for pediatric studies. Neuroimage [Internet] 2011 [cited 2020 Nov 8];54(1):313–27. Available from: https://pubmed.ncbi.nlm.nih.gov/20656036/
9. Glasser MF, Sotiropoulos SN, Wilson JA, et al. The minimal preprocessing pipelines for

the Human Connectome Project. Neuroimage [Internet] 2013 [cited 2020 Nov 8];80:105–24. Available from: https://pubmed.ncbi.nlm.nih.gov/23668970/

10. Greve DN, Fischl B. Accurate and robust brain image alignment using boundary-based registration. Neuroimage [Internet] 2009 [cited 2020 Nov 8];48(1):63–72. Available from: https://pubmed.ncbi.nlm.nih.gov/19573611/

11. Jenkinson M, Bannister P, Brady M, Smith S. Improved optimization for the robust and accurate linear registration and motion correction of brain images. Neuroimage [Internet] 2002 [cited 2020 Nov 8];17(2):825–41. Available from: https://pubmed.ncbi.nlm.nih.gov/12377157/

12. Cox RW, Hyde JS. Software tools for analysis and visualization of fMRI data. NMR Biomed [Internet] 1997 [cited 2020 Nov 8];10(4–5):171–8. Available from: https://pubmed.ncbi.nlm.nih.gov/9430344/

13. Power JD, Mitra A, Laumann TO, Snyder AZ, Schlaggar BL, Petersen SE. Methods to detect, characterize, and remove motion artifact in resting state fMRI. Neuroimage 2014;84.

14. Behzadi Y, Restom K, Liau J, Liu TT. A component based noise correction method (CompCor) for BOLD and perfusion based fMRI. Neuroimage [Internet] 2007 [cited 2020 Nov 8];37(1):90–101. Available from: https://pubmed.ncbi.nlm.nih.gov/17560126/

15. Satterthwaite TD, Elliott MA, Gerraty RT, et al. An improved framework for confound regression and filtering for control of motion artifact in the preprocessing of resting-state functional connectivity data. Neuroimage 2013;64(1).

16. Abraham A, Pedregosa F, Eickenberg M, et al. Machine learning for neuroimaging with scikit-learn. Front Neuroinform [Internet] 2014 [cited 2020 Nov 8];8(FEB):14. Available from: http://journal.frontiersin.org/article/10.3389/fninf.2014.00014/abstract

17. Woolrich MW, Ripley BD, Brady M, Smith SM. Temporal autocorrelation in univariate linear modeling of FMRI data. Neuroimage 2001;14(6).

18. Beckmann CF, Jenkinson M, Smith SM. General multilevel linear modeling for group analysis in FMRI. Neuroimage [Internet] 2003 [cited 2020 Nov 8];20(2):1052–63. Available from: https://pubmed.ncbi.nlm.nih.gov/14568475/
19. Woolrich M. Robust group analysis using outlier inference. Neuroimage 2008;41(2).
20. Woolrich MW, Behrens TEJ, Beckmann CF, Jenkinson M, Smith SM. Multilevel linear modelling for FMRI group analysis using Bayesian inference. Neuroimage 2004;21(4).
21. Worsley Keith. Statistical analysis of activation images. In: Functional MRI: An Introduction to Methods. 2001.
22. Meyer-Gerspach AC, Ly HG, Borgwardt S, et al. Endogenous GLP-1 alters postprandial functional connectivity between homeostatic and reward-related brain regions involved in regulation of appetite in healthy lean males: A pilotstudy. Diabetes, Obes Metab 2018;20(10).